Temperature dependence of viscosity in a two-dimensional dusty plasma without the effects of shear thinning

Zach Haralson and J. Goree

Citation: Physics of Plasmas **23**, 093703 (2016); doi: 10.1063/1.4962512
View online: http://dx.doi.org/10.1063/1.4962512
View Table of Contents: http://scitation.aip.org/content/aip/journal/pop/23/9?ver=pdfcov
Published by the AIP Publishing

Temperature dependence of viscosity in a two-dimensional dusty plasma without the effects of shear thinning

Zach Haralson and J. Goree
Department of Physics and Astronomy, The University of Iowa, Iowa City, Iowa 52242, USA

(Received 30 June 2016; accepted 21 August 2016; published online 14 September 2016)

An experiment was designed to measure viscosity and its temperature dependence in a two-dimensional dusty plasma. To avoid shear thinning while maintaining a uniform temperature, the shear flow and heating were provided separately, using different kinds of laser manipulation. The viscosity was found to be significantly higher than that was reported in three previous experiments most similar to ours, probably due to our avoidance of shear thinning. The viscosity increases linearly with the inverse temperature Γ, as predicted by simulations for a liquid-like strongly coupled plasma at low temperatures. *Published by AIP Publishing.* [http://dx.doi.org/10.1063/1.4962512]

I. INTRODUCTION

The shear viscosity is a transport coefficient for momentum in inhomogeneous flows. This transport coefficient, which is widely used to describe both plasmas and fluids, relates two hydrodynamic quantities: shear stress and shear rate. The shear stress P_{xy} is the off-diagonal element of a pressure tensor, and the shear rate γ is the transverse gradient of the flow velocity $\mathbf{u}$. For a flow in the y direction,

$$\gamma = \frac{\partial u_y}{\partial x}. \tag{1}$$

The shear viscosity η relates these two hydrodynamic quantities through the constitutive relation[1]

$$P_{xy} = -\eta\gamma. \tag{2}$$

In this paper, we will use Eq. (2) to determine the viscosity with an input of experimental measurements of P_{xy} and γ.

In a plasma, viscosity arises from Coulomb collisions among individual charged particles. This is so for both weakly and strongly coupled plasmas, where the particles in a strongly coupled plasma have an interparticle potential energy that is larger than the thermal kinetic energy. There is a particular interest in viscosity of strongly coupled plasmas[2,3] because they are dominated by Coulomb collisions.

Among the many types of strongly coupled plasmas, one that is especially well suited for experiments is the dusty plasma.[4–8] It consists of three familiar components of a plasma—electrons, ions, and rarefied neutral gas atoms—along with small particles of solid matter. In many experiments, the solid particles, which we term dust particles, are polymer microspheres that are introduced in a weakly ionized glow discharge plasma. A particle with a diameter of 10 μm typically collects a negative electrical charge $Q \sim -10^4\, e$, so that the dust particles repel one another strongly. This repulsion has a large potential energy so that the collection of dust particles represents a strongly coupled plasma. Another consequence of the finite size of the dust particles is that they scatter light efficiently, so that experimenters can image individual particles and track them as they move about by using video microscopy. Particle positions and velocities are obtained by analyzing video images.[9–11] These measurements are straightforward in experiments having only a single layer of dust particles, which is levitated electrically above a negatively biased horizontal electrode.[12,13] These single layers can be prepared so that out-of-plane displacements of particles are so small that they have negligible effect on the horizontal motion. In this sense, the dust cloud is essentially two-dimensional (2D). Experiments with these 2D dust clouds have verified[14] that the interparticle force is consistent with the Debye-Hückel (Yukawa) model

$$\begin{aligned} \mathbf{F}_{ij}(t) &= -\nabla\Phi_{ij}(t) \\ \Phi_{ij}(t) &= \frac{Q^2}{4\pi\epsilon_0}\frac{e^{-r_{ij}(t)/\lambda}}{r_{ij}(t)}, \end{aligned} \tag{3}$$

where $r_{ij}(t)$ is the instantaneous separation of two particles with charge Q, and λ is a screening length.

As in other strongly coupled plasmas, the particles in a dusty plasma can behave collectively like a solid or a liquid.[15] Solid-like behavior occurs when the kinetic temperature of the dust particles is low, for example, near room temperature. Under these conditions, particles arrange themselves in a crystalline lattice.[16–18] By using an auxiliary heating to raise the kinetic temperature, this crystal can be melted to make a liquid, in which the particles can move about randomly to a greater extent.[19–22]

One kind of auxiliary heating employs laser beams that move rapidly across the dust cloud. When a laser beam strikes a dust particle, it applies a radiation pressure force.[23] The movement of the laser beams is accomplished by bouncing them from scanning mirrors that are rocked back and forth by alternating voltage waveforms. In addition to heating, which is accomplished by moving the laser beams over the entire dust cloud,[24–27] it is also possible to direct the laser beams differently to cause a localized flow.[28–30] In this paper, we report an experiment with a 2D dusty plasma using one pair of laser beams to heat the dust cloud and another pair to sustain a steady shear flow. This experimental configuration allows us to measure the viscosity of the dust component using the constitutive relation, Eq. (2).

It is desirable to measure viscosity under conditions with a uniform temperature and a low shear rate because viscosity depends on these two parameters. The temperature dependence of viscosity can be very strong; for example, in motor oil, η can diminish ten-fold with only a 10% increase in the absolute temperature. Therefore, if temperature is not uniform but varies with position in a flow, one cannot obtain a single value for its viscosity. The other dependence of viscosity, on shear rate, is a non-Newtonian property of some fluids; this effect is called "shear thinning" if η diminishes with increasing γ.[31] Shear thinning can be avoided in an experiment by applying a small shear stress, so that conditions are relatively close to equilibrium.

Previous experiments[32–41] have demonstrated the usefulness of laser-driven shear flows for measuring viscosity in a dusty plasma. Three experiments[39–41] are most comparable to ours because the dust cloud had only a single layer, the kinetic temperature was well above the melting point, and the flow pattern was straight and steady. However, no auxiliary heating was used in those experiments to control temperature separately from the application of shear. Those experimenters relied instead on shear-induced melting,[38,42] which requires a strong shear stress that leads to both nonuniform temperatures and shear thinning. As a result, it is not possible to measure viscosity's dependence on temperature separately from its dependence on shear rate. The essential problem is that the temperature and shear rate increase together, when relying solely on shear-induced melting. Another problem to avoid is a shear rate that is nonuniform on the scale length of the interparticle spacing, to meet the validity requirement of the hydrodynamic approach.[1]

In this paper, we report an experiment with an upgraded apparatus allowing separate control of temperature and shear. We use two pairs of laser beams, as compared to a single pair or even just a single laser beam as in previous experiments. One pair provides auxiliary heating, allowing us to sustain a liquid with a temperature that is uniform and adjustable. The other pair drives a steady shear flow with a low shear rate that was nearly uniform in the measurement region. With this laser manipulation scheme, we will measure the viscosity and its temperature dependence without the effects of shear thinning and nonuniformities.

II. CONSTITUTIVE RELATION FOR VISCOSITY

To obtain the viscosity experimentally, using Eq. (2), requires measuring the shear stress P_{xy} and shear rate γ. In a fluid such as water, it is possible to measure both quantities using a viscometer consisting of two concentric cylindrical surfaces in contact with the fluid: the shear stress is measured from the torque exerted by a motor that drives a rotating cylinder, while the shear rate is obtained from the difference in rotational speeds of the cylinders.[31] In a dusty plasma, however, it is not possible to make these external measurements because the boundary of a dust cloud will never make contact with a solid surface in the way that water molecules can. What we can measure instead are the *in situ* particle positions and velocities, and this is done within the dust cloud's volume, not on its boundaries. These particle measurements allow us to obtain hydrodynamic quantities using equations that we list next.

In a 2D dust cloud, the areal density and the corresponding Wigner-Seitz radius are

$$n = N/A$$
$$a = (n\pi)^{-1/2}. \tag{4}$$

In our experiment, N is the number of particles counted within a camera's field of view (FOV), which has area A, and both n and a are averaged over the full time duration of an experimental run. A characteristic time scale for collective motion of the dust particles is defined by the nominal 2D dusty plasma frequency

$$\omega_{pd} = (Q^2/2\pi\epsilon_0 m a^3)^{1/2}. \tag{5}$$

The kinetic temperature, hydrodynamic flow velocity, and shear stress are

$$T = \frac{m}{2k_B}\langle \tilde{\mathbf{v}}_i(\mathbf{x}_i,t)^2\rangle, \tag{6}$$

$$\mathbf{u} = \langle \mathbf{v}_i(\mathbf{x}_i,t)\rangle, \tag{7}$$

$$P_{xy} = \frac{1}{A}\left\langle \sum_i m\tilde{v}_{i,x}\tilde{v}_{i,y} + \frac{1}{2}\sum_i\sum_{j\neq i} r_{ij,y}F_{ij,x}\right\rangle, \tag{8a}$$

$$= \frac{m}{A}\left\langle \sum_i \tilde{v}_{i,x}\tilde{v}_{i,y} + \frac{a^3\omega_{pd}^2}{4} \times \sum_i\sum_{j\neq i} r_{ij,y}\left[\frac{\mathbf{r}_{ij}}{r_{ij}^2}e^{-r_{ij}/\lambda}\left(\frac{1}{r_{ij}}+\frac{1}{\lambda}\right)\right]_x\right\rangle. \tag{8b}$$

Here, $\mathbf{x}_i$ and $\mathbf{v}_i$ are the instantaneous position and velocity of particle i, $\tilde{\mathbf{v}}_i(\mathbf{x}_i,t) = \mathbf{v}_i(\mathbf{x}_i,t) - \mathbf{u}$, and m is the particle mass. The subscripts x and y in Eq. (8) denote vector components. The expression in Eq. (8b) makes use of Eqs. (3) and (5). We will compute P_{xy} using pairs of particles separated by a distance r_{ij}, up to a maximum radius where we cut off, $r_{\text{cut}} = 6\lambda$.

Obtaining the shear stress P_{xy} from experimental data requires the particle positions and velocities, as well as the interaction force $\mathbf{F}_{ij}$. Like previous experimenters,[40] we cannot measure this force directly; instead, we calculate it from the particle positions using the Debye-Hückel expression, Eq. (3), with values for Q and λ that must be obtained empirically.

When we perform the averages in Eqs. (6)–(8) denoted by brackets $\langle\,\rangle$, we will exploit the steady straight flow conditions of our experiment. These steady conditions will allow us to average over the entire time duration of an experimental run. The spatial symmetry provided by the straight flow allows us to average over the ignorable y direction. We do this spatial averaging within bins centered at specified values x, which should not be confused with the instantaneous position $\mathbf{x}_i(t)$ of a particle. After performing these averages $\langle\,\rangle$, the hydrodynamic quantities defined in Eqs. (6)–(8) will be expressed as spatial profiles $T(x)$, $\mathbf{u}(x)$, and $P_{xy}(x)$. We also require a profile $\gamma(x)$ calculated from $\mathbf{u}(x)$ using Eq. (1).

From the profiles for P_{xy} and γ, we can obtain the viscosity η using the constitutive relation, Eq. (2), rewritten as

$$\eta = -P_{xy}/\gamma\,. \tag{9}$$

This viscosity describes the momentum transport for only the dust component of the dusty plasma. Unlike a colloid, for example, a dusty plasma does not have a single viscosity for the entire fluid. This is the case because a dusty plasma is highly rarefied, so that dust particles are not overdamped by friction on the other components (gas, electrons, and ions).[43] Thus, the dust particles can move collectively with a flow velocity that is different from the average velocities of the other plasma components. This different flow velocity means that momentum in the dust component is described by a transport coefficient that is separate from those of the electrons, ions, and gas. The temperature of the dust component can also be different.

We note that Eqs. (6)–(9) convert from a particle description to a hydrodynamic description of the dust cloud. The validity of this hydrodynamic description and its viscosity coefficient can be confirmed by examining the experimental results of Ref. 44. In that experiment, it was verified that the momentum and energy equations are simultaneously balanced in a 2D dusty plasma with a shear flow. Our experiment, reported here, should likewise have a valid hydrodynamic description of dust momentum because we will use weaker gradients than in Ref. 44.

In this paper, we will use several dimensionless parameters. We normalize lengths by a and time by ω_{pd}. For Yukawa systems, the screening length is often expressed as the dimensionless screening parameter[3]

$$\kappa = a/\lambda\,. \tag{10}$$

In the literature for strongly coupled plasmas, the inverse temperature is commonly expressed as the dimensionless Coulomb coupling parameter,[45]

$$\Gamma = \frac{Q^2}{4\pi\epsilon_0 a k_B T}\,, \tag{11}$$

where $\Gamma \gg 1$ in a strongly coupled plasma. The shear rate γ can be normalized[46] using the Wigner-Seitz radius a and the thermal velocity $v_{\rm th} = (2k_BT/m)^{1/2}$ to give

$$\bar{\gamma} = \gamma(a/v_{\rm th})\,. \tag{12}$$

According to the simulation results of Ref. 46, significant shear thinning will occur for $\bar{\gamma} \geq 0.2$ in a 2D dusty plasma such as ours. Viscosity can also be normalized, in two steps. First, we divide viscosity by the areal mass density $\rho = mn$ to yield a kinematic viscosity, which has been reported[39,41] to be on the order of 1 mm^2/s for 2D dusty plasmas. Second, we divide by $a^2\omega_{pd}$, yielding

$$\bar{\eta} = \eta/(\rho a^2\omega_{pd}), \tag{13a}$$

$$= -\frac{\pi}{A\gamma}\left\langle \frac{1}{\omega_{pd}}\sum_i \tilde{v}_{i,x}\tilde{v}_{i,y} + \frac{a^3\omega_{pd}}{4} \times \sum_i \sum_{j\neq i} r_{ij,y}\left[\frac{\mathbf{r}_{ij}}{r_{ij}^2}e^{-r_{ij}/\lambda}\left(\frac{1}{r_{ij}}+\frac{1}{\lambda}\right)\right]_x\right\rangle. \tag{13b}$$

The diameter of the dust particles affects this expression only indirectly through ω_{pd}, which is proportional to $Q/\sqrt{m}$ in Eq. (5). Usually, a particle's charge and mass are proportional to the first and third powers of its diameter, respectively, so that ω_{pd} is only weakly dependent on the particle diameter. Thus, Eq. (13b) for the normalized viscosity is not highly sensitive to the particle size.

III. LASER MANIPULATION FOR SIMULTANEOUS HEATING AND SHEAR

Laser manipulation serves two roles in an experiment such as ours. It provides heating, which melts a crystal and sustains liquid conditions. It also drives a macroscopic flow, in which the dust particles circulate in a pattern that includes a region of straight shear flow. As discussed above, it is possible to achieve both liquid conditions and a shear flow with only shear manipulation, although with some limitations since each laser beam is filling dual roles.

We next describe our experimental design, which was specifically configured to provide improved viscosity measurements through the use of separate heating and shear. To accomplish this, we used one pair of laser beams to provide heating as we did in Ref. 27, and we have now added a separate pair to drive the shear, as sketched in Fig. 1. This manipulation scheme allowed us to achieve the two desirable conditions mentioned previously: a spatially uniform temperature and a low shear rate.

To achieve a uniform temperature profile, the heating laser beams were applied to a rectangular "heating region" large enough to include the entire dust cloud, as sketched in Fig. 2. The power of a 532 nm laser was varied up to 18 W to adjust the temperature. This laser's beam was split into two, and the resulting beams were focused and then pointed by pairs of galvanometer scanning mirrors. These mirrors tilted back and forth in response to the voltage waveforms, causing

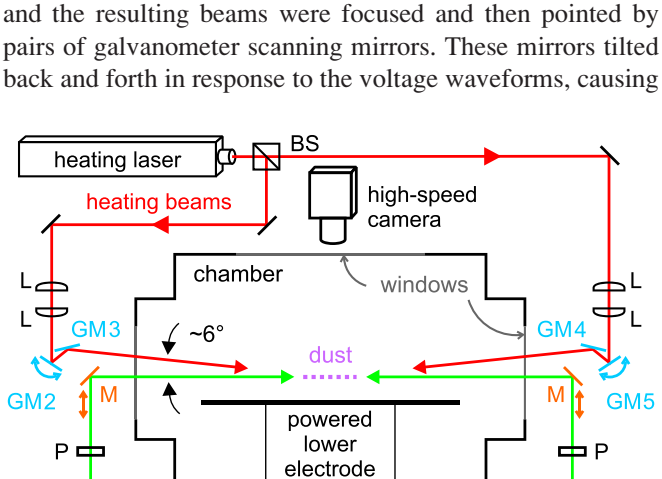

FIG. 1. Side-view sketch of our apparatus. To allow simultaneous heating and shear, two lasers were used to generate two separately controlled pairs of beams. A single layer of dust particles was levitated above the powered lower electrode, and the particle motion was recorded by a high-speed camera viewing from above. Optical components are: BS cube beamsplitter, L positive spherical lens, GM galvanometer scanning mirror, M mirror at an adjustable height, P rotatable polarizer, and CL positive cylindrical lens. Another laser sheet, for illuminating the particles, is not shown here.

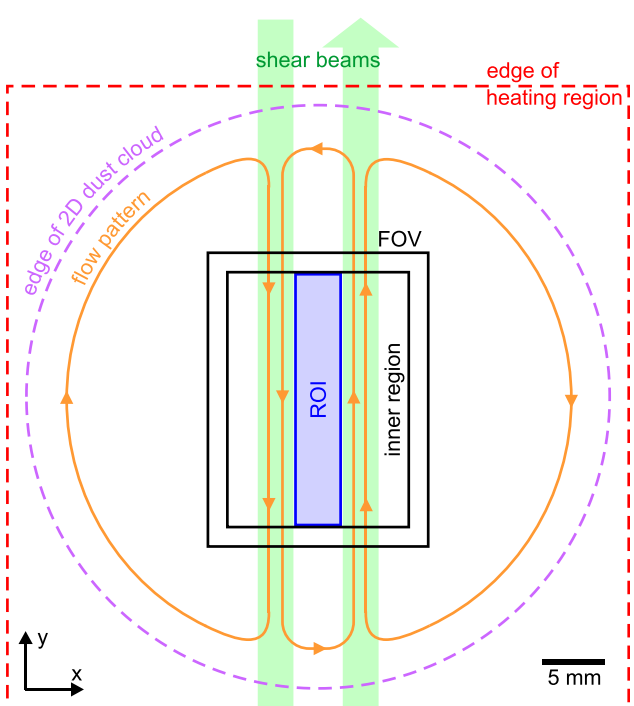

FIG. 2. Top-view sketch of the laser manipulation scheme. To achieve a uniform temperature, the dust cloud lay entirely within the rectangular "heating region," where the pair of heating beams moved back and forth. To achieve a steady straight shear flow without shear thinning, a shear laser operating at a low power of 118 mW was split to form two shear beams, shown as thick arrows. The flow pattern of dust particles, as sketched here, recirculated in a pattern of three vortices, elongated so that the flow pattern was straight within the camera's field of view (FOV), which was 17.6×23.4 mm. Particles within the "inner region" of the FOV were used to obtain spatial profiles of hydrodynamic quantities. Viscosity values obtained in the smaller region of interest (ROI) will be our main result.

the two heating beams to move across the dust cloud. When a beam struck a dust particle, it imparted some momentum to the particle, and this input of momentum was thereafter randomized by collisions with other dust particles. Further details of this heating configuration and laser beam movement are described in Ref. 27.

To drive a straight and steady shear flow with the desired low shear rate, the shear beams were shaped like horizontal ribbons and directed onto the dust cloud in opposite directions. These shear beams were added to our apparatus especially for the experiment reported in this paper. The resulting flow pattern, sketched in Fig. 2, consisted of three circulations that were elongated so that the flow velocity was straight in the gap between the beams. Microparticles located within this gap will be of greatest interest in our analysis of viscosity.

The optics to produce the ribbon-shaped shear beams are shown in Fig. 1. The shape of the beam was defined before it was split. The beam was spread into a fan using a scanning mirror GM1 operated at 30 Hz, and it was then collimated by a pair of convex cylindrical lenses CL. We chose our configuration, with the scanning mirror and collimating lenses, because we found that it resulted in a uniform laser intensity across the ribbon's width.

To control the shear profile precisely, three parameters could be selected: the gap between beams, ribbon width, and intensity. We adjusted the gap using mirrors mounted on translation stages with motorized actuators, not shown in Fig. 1. The width was adjusted by varying the amplitude of the waveform applied to the galvanometer scanning mirror GM1. The intensity was chosen by adjusting the 532 nm laser's power up to 500 mW. For this experiment, we chose the gap to be 4.0 mm, the ribbon width to be 3.5 mm, and the laser power to be 118 mW. This laser was linearly polarized, allowing us to balance the intensity of the two shear beams by rotating polarizers P. To align the ribbon-shaped shear beams so that they lay in the same plane as the razor-thin dust cloud, we adjusted each beam's height and tilt using two translation stages for mirrors M. The thickness of the beams, which was fixed at 1.2 mm, was large enough to ensure that particles were illuminated equally within a stripe across the dust cloud.

IV. EXPERIMENT

A. Procedure

A partially ionized argon plasma was sustained using the capacitively coupled rf power. We applied 13.56 MHz power to a horizontal lower electrode, while the vacuum chamber, shown in Ref. 47, served as the grounded electrode. To ensure that it remained steady during the seven hours of observations, the argon gas pressure was regulated at 6.0 mTorr by a feedback controller with a temperature-stabilized capacitance manometer pressure sensor. During this long observation period, although the peak-to-peak voltage on the lower electrode remained steady at 112 V, the dc self-bias drifted downward 8% from −75 to −69 V. Our tests suggest that this drift might be due to a slight trend in the gas purity that occurs in the presence of the dust, perhaps due to outgassing or sputtering.

The dust particles were confined in a single layer. There was no significant out-of-plane motion, which we verified using a side-view camera. For this experiment, the particles were melamine formaldehyde (MF) microspheres. We introduced about 6000 particles using a dispenser located above the plasma. The cloud of particles settled in a single layer, which was confined in the radial direction to have a diameter of about 5 cm. The manufacturer of the MF particles specified their diameter and mass as 8.69 μm and $m = 5.2 \times 10^{-13}$ kg, respectively.

The particle mass can diminish during the experiment, but this has only a small effect on our result for the normalized viscosity. Previous experimenters using the same kind of MF particles[48–50] have observed a mass loss during storage in vacuum conditions and during exposure to a plasma.[51] If this process could also result in a diminishing particle diameter, we expect that Q would diminish in proportion. Fortunately, for our experiment, any small changes in particle mass and charge will have little effect on our result for the normalized viscosity, Eq. (13b), as discussed at the end of Sec. II.

Imaging of the 2D dust cloud was performed from above using a Phantom Miro M120 video camera at 70 frames/s. The corresponding time interval was $\Delta t = 14.29$ ms. We recorded 4382 frames in each run.

Three kinds of runs were performed in our experiment: crystal, shear-free liquid, and sheared liquid. Each run was

recorded as a single video. The crystal runs, which used no laser manipulation, provide the data needed to measure ω_{pd} and κ. To account for any small drifts in these two parameters, we performed crystal runs at the beginning and end of the entire experiment. In all other runs laser heating was used, with five runs at each of eight different laser powers. The five runs consisted of one shear-free run and four sheared runs. The sheared runs used the shear beams in addition to the heating beams, and they provide the main results of this paper.

To illustrate how particle motion is different in these three kinds of runs (crystal, shear-free, and sheared), Fig. 3 shows the paths of individual particles. The tracks shown reveal the particle motion during a 0.5 s time interval. In the crystal runs, the particle motion is so slight that the displacement is almost imperceptible over this time interval in Fig. 3(a). In the sheared runs, the velocities for random thermal motion and shear flow are comparable, as can be seen by the lengths of the streaks in Fig. 3(c).

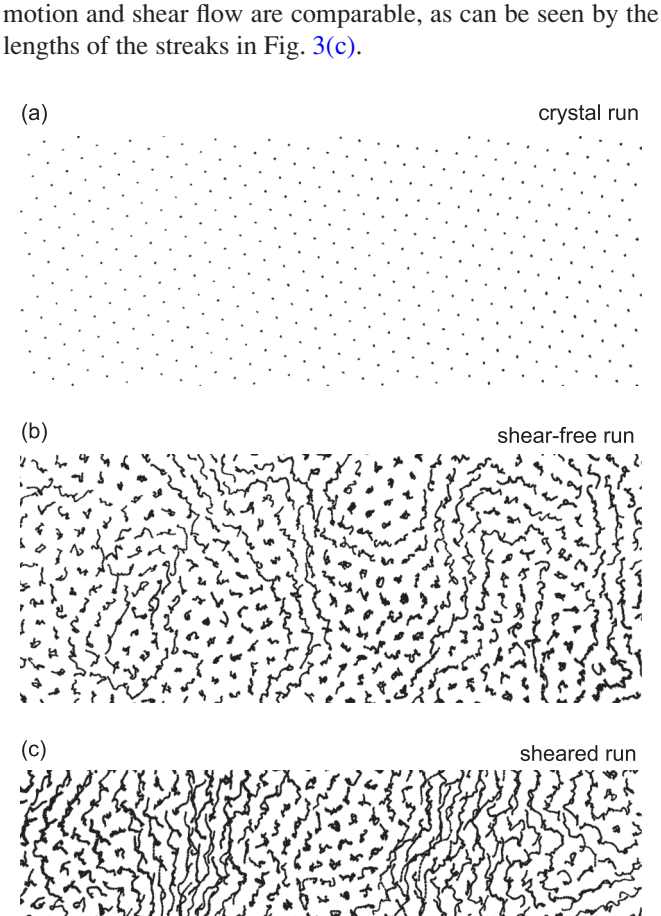

FIG. 3. Particle trajectories showing the paths of individual particles in the 2D layer. Images shown here were made by superimposing video frames recorded during 0.5 s. (a) In a crystal run, the particles were self-organized with equilibrium positions arranged in a triangular lattice. The particles moved minutely, but the image analysis methods allowed tracking particle motion in this crystal to obtain the particle charge Q and screening length λ. In other runs, cold liquid conditions were achieved by applying laser heating to enhance the random motion of the dust particles, as shown by the trajectories in (b). In (c), shear beams were also applied; the trajectories reveal a combination of random thermal motion and a shear flow. Images shown here were cropped, they do not show the entire FOV.

The shear-free runs allowed us to verify that the particle motion mimicked a thermal equilibrium. This verification consisted of two tests. First, we verified that the velocity distribution function is nearly Maxwellian with a q value[52] of $\approx$1.07, as compared to unity for a true Maxwellian. Second, we compared the rms fluctuations of the time series for the kinetic temperature of a finite number of particles to the expected value for a canonical ensemble in thermal equilibrium. We found that the temperature fluctuations in our experiment were 1.5 times the canonical temperature fluctuations. This multiple is somewhat higher than in the ideal case of numerical simulations,[53] but it is typical for experiments with laser-heated dusty plasmas.[25]

B. Particle and hydrodynamic measurements

We now describe how we obtained the inputs required to measure viscosity with Eqs. (7)–(9) and temperature using Eq. (6). The first group of inputs consists of particle positions and velocities, measured directly from video data. The second group of inputs is ω_{pd} and κ, which we obtained using the standard phonon spectrum method. The third group consists of the spatial profiles of hydrodynamic quantities, which were calculated by spatial and temporal averaging of particle data. Details of the calculations for these groups of data are presented next.

1. Particle positions and velocities

Particle positions from our images are our primary measurement. We used them to obtain the particle velocities as we describe below, the interparticle forces using Eq. (3), and the Wigner-Seitz radius using Eq. (4). We also used them to assign particles to bins when we prepared spatial profiles $T(x)$, $\mathbf{u}(x)$, and $P_{xy}(x)$.

The position of an individual particle was measured using an optimized moment method.[9,11] This method uses the intensity in each pixel. In our experiment, a particle's image filled about 20–25 pixels. We repeated this measurement of particle coordinates in each of the 4382 video frames per run. In each frame, typically about 1400 particles appeared in the camera's FOV, so that altogether we made more than 10^6 particle measurements in each run.

After measuring the particle positions, we obtained their velocities using the particle tracking velocimetry method.[10,11] For each particle identified in frame k, we searched a 20 pixel radius[54] in the next frame $k+1$ to identify the same particle. We then calculated its velocity simply as the change in position divided by the time Δt between frames. Thus, the velocities were recorded at times $(k+0.5)\Delta t$, while the positions were recorded at different times, $k\Delta t$. The inputs for the instantaneous shear stress P_{xy} in Eq. (8) include both particle positions and velocities; for this purpose, we interpolated two consecutive position measurements so that we obtained P_{xy} at time $(k+0.5)\Delta t$ using inputs for that specific time.

While the particle measurements are our most precise data, they are subject to errors which affect the rest of our analysis. For the particle position measurements, we assessed the random and systematic errors and determined that the largest uncertainty was a ± 0.5 pixel systematic error in the x coordinate of a particle, due to an imaging artifact. This

artifact was a triangular distortion of each particle's image arising from an asymmetry in a filter aperture. In a test, we verified that this systematic error had a negligible effect on our final value for the viscosity. This test was performed by adding additional Gaussian random errors, with an rms value of 0.5 pixel, and repeating the entire analysis. To achieve high precision in the velocity measurements, we operated with a combination of lower flow velocity and higher frame rate, as compared to some previous experiments.[39,40]

These measurements of particle position and velocity are the basis of all our analysis. Depending on the quantity being calculated, we used either all the particles located in the camera's FOV, or only those in a smaller "inner region." The inner region excluded from the FOV a narrow border of width r_{cut} all the way around its perimeter, as shown in Fig. 2. The quantities that we obtained using the entire FOV are n, a, ω_{pd}, and κ. For the hydrodynamic quantities, we used the smaller inner region for particles denoted as i in Eqs. (6)–(8), but the full FOV for particles denoted as j in Eq. (8) for P_{xy}. By limiting i to the inner region in Eq. (8), we retained all the interparticle interactions up to the cutoff radius r_{cut}.

2. Determination of ω_{pd} and κ

We require experimentally measured values for ω_{pd} and κ to calculate P_{xy} using Eq. (8b). For this purpose, we used data from our crystal runs in the standard method of fitting phonon spectra. This method required first calculating a transverse current from the positions and velocities of all particles j in the FOV. We then calculated the Fourier transform of this current to yield two experimental spectra, for longitudinal and transverse motion.[55,56] Both spectra were then fit to theoretical dispersion relations for Yukawa particles on an ideal triangular lattice;[57] we obtained ω_{pd} and κ as the two free parameters in this fit.

Our fit results were $\omega_{pd} = 86\,\mathrm{s}^{-1}$ and $\kappa = 0.72$ at the beginning of the experiment. These values drifted about 7%, so that at the end of the experiment, they were $92\,\mathrm{s}^{-1}$ and 0.78, respectively. All the results reported hereafter will use values of ω_{pd} and κ interpolated linearly with time between these starting and ending values.

The uncertainties in ω_{pd} and κ can be seen in the χ^2 contours of Fig. 4. We used these contours to obtain not only the best fit, which is the central minimum, but also to determine the one-sigma uncertainty, corresponding to the outermost contour shown.[58] This error propagates into the determination of P_{xy} using Eq. (8) and therefore contributes an error to $\bar{\eta}$; we determined[59] this error to be less than 10%. We believe that this error is the largest of all contributions to the uncertainty in our results for $\bar{\eta}$.

The Wigner-Seitz radius was $a = 0.307\,\mathrm{mm}$ at the beginning of the experiment. We measured a separately in every video, and found that the particle spacing gradually diminished, so that $a = 0.298\,\mathrm{mm}$ at the end of the experiment.

The charge, calculated from the separate measurements of ω_{pd} and a, was $-15\,500\,e$ at the beginning of the experiment. Due to the offsetting trends of ω_{pd} and a, we found that Q was more nearly constant than other particle parameters, ending the experiment at $Q = -15\,900\,e$, assuming a constant mass.

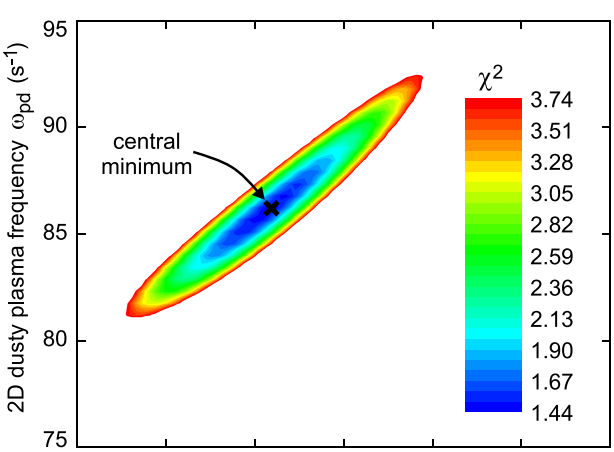

FIG. 4. Contours of χ^2 as a function of two fitting parameters, ω_{pd} and κ. This fitting of the theoretical dispersion relation to experimental spectra allows us to obtain the particle charge and screening length. Data shown are for the crystal run at the start of our experiment. The best fit is at the central minimum, while uncertainties at a 68.3% confidence level (one-sigma) are indicated by the outermost contour, for an increase of 2.30 in χ^2.

3. Converting particle data to hydrodynamic profiles

Obtaining the viscosity as a function of temperature required converting our particle-level data for positions and velocities into hydrodynamic quantities for the dust component using Eqs. (6)–(8). The averages denoted by brackets $\langle\,\rangle$ in these equations consist of both temporal and spatial averaging. For the temporal averaging, we exploited the steady condition of the shear flow by averaging over an entire run. For the spatial averaging, we used binning.

The spatial binning was designed to provide the required spatial resolution while exploiting the symmetry of the experiment. The symmetry of the flow pattern arose from the straightness of the flow within the FOV, where the flow velocity $\mathbf{u}$ was only in the y direction, i.e., $\mathbf{u} = u_y(x)\hat{y}$. This symmetry allowed using bins that were long in the y direction but narrow in the x direction. In fact, in the y direction, our bins traversed the entire inner region of Fig. 2. In the x direction, the bins had a narrow width that we chose as $\Delta x = 0.314\,\mathrm{mm} \approx a$. This width was chosen as a tradeoff to provide sufficient spatial resolution while also providing enough particles per bin, which on average was 41.8, to allow good statistics.

Assigning particles to bins required a specified weighting of the particles. Rather than "nearest grid-point" weighting, which assigns an entire particle to a single bin l, we used the smoother "cloud-in-cell" weighting.[60] This weighting distributes a particle's contribution between two bins, so that quantities do not change abruptly as a particle moves from one bin to another.

V. HYDRODYNAMIC PROFILE RESULTS

As a step toward our main result, which will be the viscosity and its temperature dependence, we present in Fig. 5

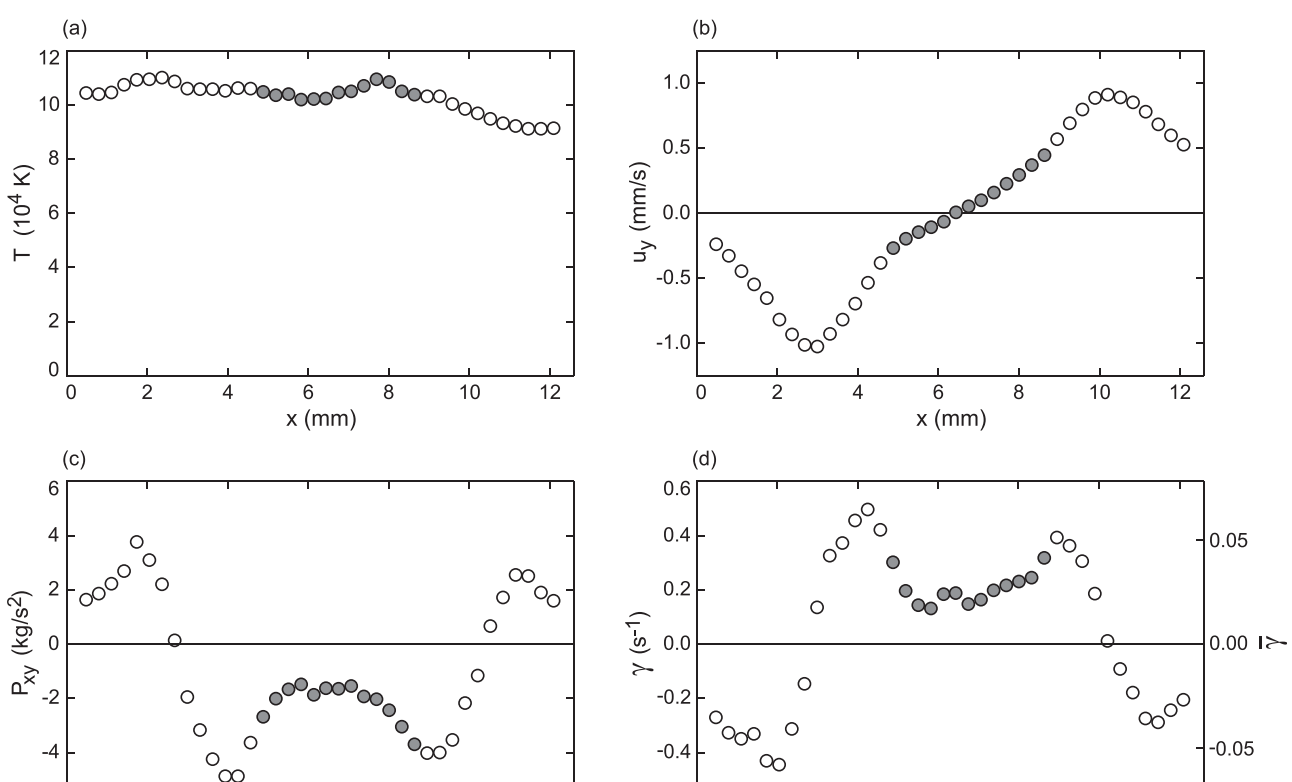

FIG. 5. Spatial profiles, for a representative sheared run, showing (a) the kinetic temperature T from Eq. (6), (b) the flow velocity u_y from Eq. (7), (c) the shear stress P_{xy} from Eq. (8), and (d) the shear rate γ from Eqs. (1) and (12). These profiles were obtained with an input of data for particle positions and velocities, and they were averaged over spatial bins and time. The data shown span the entire width of the "inner region" of Fig. 2; the ROI is indicated by filled data points. Within the ROI, the temperature profile in (a) has a high degree of uniformity, with variations of only $\pm 5\%$, while the shear rate in (d) meets the requirement $\bar{\gamma} < 0.2$ for shear thinning to be insignificant.

profiles of four hydrodynamic quantities for a representative sheared run. These profiles show the kinetic temperature $T(x_l)$, flow velocity $u_y(x_l)$, and shear stress $P_{xy}(x_l)$, calculated using Eqs. (6)–(8) in a bin l centered at x_l. Also presented in Fig. 5(d) are the shear rate $\gamma(x_l) = (u_y(x_{l+1}) - u_y(x_{l-1}))/2\Delta x$ and the normalized shear rate $\bar{\gamma}(x_l)$, calculated using Eq. (12).

The shear rate was small enough to avoid shear thinning within the region of interest (ROI). The normalized shear rate is only $\bar{\gamma} \approx 0.027$ in Fig. 5(d), which is well below the level of 0.2 for shear thinning to occur according to simulation.[46] Previous experimenters generally used much higher shear rates, with $\bar{\gamma}$ as high as 1.2 in Ref. 40 and as high as 0.7 in Ref. 41, according to our estimation.

The temperature profile is uniform across the ROI to within $\pm 5\%$. This is true for the run shown in Fig. 5(a), and for all our other sheared runs as well. This uniformity represents an improvement of two orders of magnitude over the experiments of Refs. 39 and 41, for example, where the temperature varied by a factor of three across the flows. It is useful that we attained a flat temperature profile so that we can report a single value for the viscosity in each run.

The conditions for all of our runs, except one, corresponded to a cold liquid. Our dust cloud had an absolute temperature above the melting point, but not twice as high. Equivalently, the cloud had Γ less than the melting point Γ_m, but within a factor of two of that point. For our experiment, the value of the melting point Γ_m is predicted to be in the range 155–159 depending on κ, based on Eqs. (3) and (4) of Ref. 61, combined with their Fig. 6. Thus, our conditions were in the range $0.59 < \Gamma/\Gamma_m < 0.98$. The exception was our coldest run, which had $\Gamma/\Gamma_m = 1.09$ and $\Gamma = 170$. The reason that we did not operate at higher temperatures is that we sought to achieve a uniform temperature profile, which required distributing the laser heating power over a wide heating region.[62]

One limitation of our experiment is that the random particle motion was anisotropic, as it was in previous experiments that used a pair of laser beams for heating.[25,27] The variance of $\tilde{v}_{i,y}$ was larger than that of $\tilde{v}_{i,x}$ by a ratio of about 1.4, which is an improvement over the anisotropy ratio in our previous test.[27] Values we report for Γ are based on T, computed as in Eq. (6) using both the x and y components of $\tilde{\mathbf{v}}_i$.

VI. VISCOSITY RESULTS

To obtain the viscosity for each sheared run, first we calculated the ratio $-P_{xy}/\gamma$ locally from the profiles of P_{xy} and γ. This ratio is presented as a profile for a representative run in Fig. 6. We will focus our attention on the 13 filled data points in the ROI, where this ratio varies only $\pm 15\%$. Second, exploiting this uniformity and making use of the constitutive relation Eq. (9), we obtained a single value for viscosity η in our flow as the spatial average of $-P_{xy}/\gamma$

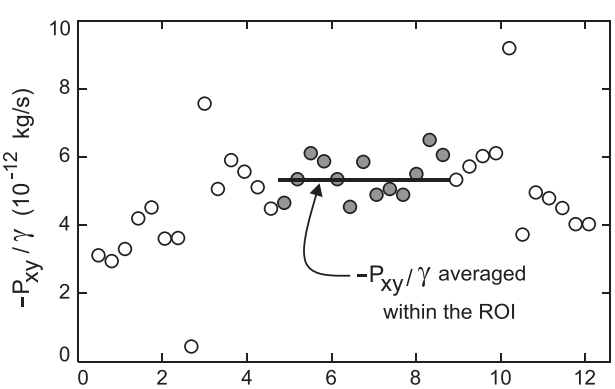

FIG. 6. Spatial profile of $-P_{xy}/\gamma$, obtained from the P_{xy} and γ profiles of Fig. 5. We will report a single value for the viscosity by averaging this ratio within the ROI, where it varies only about ±15%. The ROI is indicated by filled data points.

within the ROI. We also averaged the temperature within the ROI, so that we obtained a single value of Γ for each run as well.

Our main result is the temperature dependence of the viscosity, Fig. 7. Each data point represents one run. The trend shown in Fig. 7 is that the viscosity increases with Γ; in other words, viscosity increases with decreasing temperature. Our data fit a straight line

$$\bar{\eta} = 0.0265 + 0.00243\Gamma, \tag{14}$$

with an adjusted R^2 of 0.88. We expect that the two fit coefficients in Eq. (14) should in general depend on κ, but our κ varied so little that we are able to fit all our data to a single line. We note that the linear form of Eq. (14) is not just a result peculiar to our experiment; it is actually a special case of the more general empirical form,

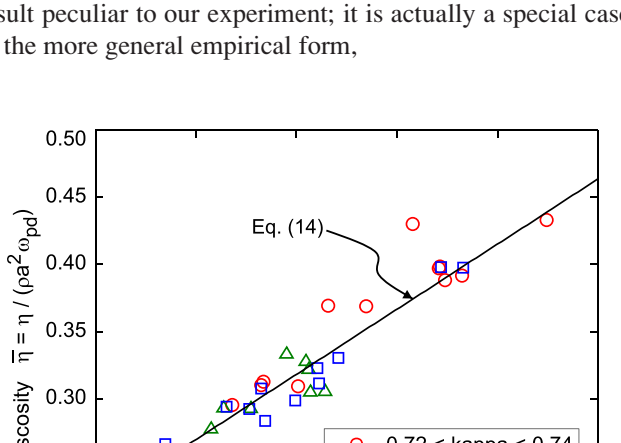

FIG. 7. Kinematic viscosity versus inverse temperature, both in dimensionless units. For each data point, corresponding to one experimental run, the viscosity shown is the spatial average of $-P_{xy}/\gamma$ within the ROI as described in Fig. 6, while Γ is obtained from Eq. (11). The data fit a straight line, Eq. (14). The main uncertainty for the x axis is a systematic error arising from the determination of ω_{pd}; this uncertainty could cause the entire data set shown here to be shifted right or left by ±16, in the value of Γ. Uncertainties for the y axis include random errors of about ±7% in the value of the viscosity as indicated by the scatter, as well as systematic errors of <10% arising from the determination of ω_{pd}.

$$a + b\Gamma + c/\Gamma, \tag{15}$$

often used to describe the temperature dependence of viscosity obtained from simulations.[2,46] Our value of Γ was high enough that the fit is not improved by including the last term of Eq. (15), that is why we retain only the first two terms in our fit of Eq. (14).

Comparing to simulations of Yukawa liquids,[2,46,63–65] we observe that the trend of our data agrees with the predicted monotonic increase of $\bar{\eta}$ with Γ at low temperatures. These simulations, which have been performed over much wider temperature ranges than we could achieve, predict that viscosity also increases at high temperatures, so that there is a minimum viscosity at a particular intermediate temperature. The minimum viscosity, predicted at Γ of about 20, corresponds to $\Gamma_{\min} = \sqrt{c/b}$ in Eq. (15). Our experiment did not extend to the high temperatures needed to observe this minimum.

In addition to the similar trend, our viscosity data also show similar values to simulations. In particular, our experimental viscosity values for $\kappa \approx 0.75$ lie between the simulation values for $\kappa = 0.5$ and $\kappa = 1.0$ in Ref. 46. In that simulation, a non-equilibrium method was used, with an applied shear that was weak enough to avoid the effects of shear thinning.

Compared to three similar previous experiments,[39–41] we find that our viscosity values are generally higher, by a factor as large as two. We attribute this difference to the design of our experiment and our avoidance of shear thinning. In support of this argument, we note that among the previously reported values, the closest to ours are the several highest viscosity data points on the left side of Fig. 4 of Hartmann *et al.*,[40] recorded at the locations far from the shear beam, where the shear rate was the lowest.

VII. SUMMARY

We performed an experiment to measure viscosity and its temperature dependence in a 2D dusty plasma with a steady straight shear flow. We used separate pairs of laser beams for heating and shear, allowing us to maintain temperature uniformity while avoiding excessive shear rates. The heating beams provided liquid-like conditions with a temperature that varied only ±5% in the ROI. The shear beams drove a flow that had a shear rate of typically $\gamma \approx 0.20\,\mathrm{s}^{-1}$, corresponding to a normalized value $\bar{\gamma} \approx 0.027$. This low shear rate allowed us to avoid shear thinning.

We obtained the viscosity from the constitutive relation, Eq. (2). To investigate the viscosity's temperature dependence, we varied the heating laser power over eight levels, while the shear laser power was maintained at the same low value throughout all experimental runs.

Our results for the temperature dependence of viscosity are presented in Fig. 7. We find a trend of viscosity increasing with Γ, as predicted by simulations for low-temperature liquid conditions in a strongly coupled plasma. Our viscosity values are significantly higher than reported in previous experiments, probably due to our avoidance of shear thinning.

ACKNOWLEDGMENTS

This work was supported by the U.S. Department of Energy, the National Science Foundation, and NASA.

[1]J.-P. Hansen and I. R. McDonald, *Theory of Simple Liquids*, 2nd ed. (Academic Press, New York, 1986).
[2]T. Saigo and S. Hamaguchi, "Shear viscosity of strongly coupled Yukawa systems," Phys. Plasmas **9**, 1210–1216 (2002).
[3]Z. Donkó, P. Hartmann, and J. Goree, "Shear viscosity of strongly-coupled two-dimensional Yukawa liquids: Experiment and modeling," Mod. Phys. Lett. B **21**, 1357–1376 (2007).
[4]P. M. Bellan, "Dusty plasmas," in *Fundamentals of Plasma Physics* (Cambridge University Press, New York, 2006), Chap. 17, p. 559.
[5]A. Melzer and J. Goree, "Fundamentals of dusty plasmas," in *Low Temperature Plasmas: Fundamentals, Technologies and Techniques*, 2nd ed., edited by R. Hippler, H. Kersten, M. Schmidt, and K. H. Schoenbach (Wiley-VCH, Weinheim, 2008), Chap. 6, p. 129.
[6]G. E. Morfill and A. V. Ivlev, "Complex plasmas: An interdisciplinary research field," Rev. Mod. Phys. **81**, 1353–1404 (2009).
[7]A. Piel, "Dusty plasmas," in *Plasma Physics: An Introduction to Laboratory, Space, and Fusion Plasmas* (Springer-Verlag, Heidelberg, 2010), Chap. 10, p. 260.
[8]M. Bonitz, C. Henning, and D. Block, "Complex plasmas: A laboratory for strong correlations," Rep. Prog. Phys. **73**, 066501 (2010).
[9]Y. Feng, J. Goree, and B. Liu, "Accurate particle position measurement from images," Rev. Sci. Instrum. **78**, 053704 (2007).
[10]Y. Feng, J. Goree, and B. Liu, "Errors in particle tracking velocimetry with high-speed cameras," Rev. Sci. Instrum. **82**, 053707 (2011).
[11]Y. Feng, J. Goree, Z. Haralson, C.-S. Wong, A. Kananovich, and W. Li, "Particle position and velocity measurement in dusty plasmas using particle tracking velocimetry," J. Plasma Phys. **82**, 615820303 (2016).
[12]A. Douglass, V. Land, K. Qiao, L. Matthews, and T. Hyde, "Determination of the levitation limits of dust particles within the sheath in complex plasma experiments," Phys. Plasmas **19**, 013707 (2012).
[13]J. D. Williams, E. Thomas, L. Couëdel, A. V. Ivlev, S. K. Zhdanov, V. Nosenko, H. M. Thomas, and G. E. Morfill, "Kinetics of the melting front in two-dimensional plasma crystals: Complementary analysis with the particle image and particle tracking velocimetries," Phys. Rev. E **86**, 046401 (2012).
[14]U. Konopka, G. E. Morfill, and L. Ratke, "Measurement of the interaction potential of microspheres in the sheath of a rf discharge," Phys. Rev. Lett. **84**, 891–894 (2000).
[15]H. Thomsen, J. Schablinski, and M. Bonitz, "Phase transitions in dusty plasmas," in *Complex Plasmas: Scientific Challenges and Technological Opportunities*, edited by M. Bonitz, J. Lopez, K. Becker, and H. Thomsen (Springer International Publishing, New York, 2014), p. 3.
[16]J. H. Chu and I. Lin, "Direct observation of Coulomb crystals and liquids in strongly coupled rf dusty plasmas," Phys. Rev. Lett. **72**, 4009–4012 (1994).
[17]Y. Hayashi and K. Tachibana, "Observation of Coulomb-crystal formation from carbon particles grown in a methane plasma," Jpn. J. Appl. Phys., Part 2 **33**, L804 (1994).
[18]H. Thomas, G. E. Morfill, V. Demmel, J. Goree, B. Feuerbacher, and D. Möhlmann, "Plasma crystal: Coulomb crystallization in a dusty plasma," Phys. Rev. Lett. **73**, 652–655 (1994).
[19]H. M. Thomas and G. E. Morfill, "Melting dynamics of a plasma crystal," Nature **379**, 806–809 (1996).
[20]A. Melzer, A. Homann, and A. Piel, "Experimental investigation of the melting transition of the plasma crystal," Phys. Rev. E **53**, 2757–2766 (1996).
[21]R. A. Quinn and J. Goree, "Experimental test of two-dimensional melting through disclination unbinding," Phys. Rev. E **64**, 051404 (2001).
[22]T. E. Sheridan, "Melting transition in a two-dimensional complex plasma heated by driven acoustic instability," Phys. Plasmas **15**, 103702 (2008).
[23]B. Liu, J. Goree, V. Nosenko, and L. Boufendi, "Radiation pressure and gas drag forces on a melamine-formaldehyde microsphere in a dusty plasma," Phys. Plasmas **10**, 9–20 (2003).
[24]M. Wolter and A. Melzer, "Laser heating of particles in dusty plasmas," Phys. Rev. E **71**, 036414 (2005).
[25]V. Nosenko, J. Goree, and A. Piel, "Laser method of heating monolayer dusty plasmas," Phys. Plasmas **13**, 032106 (2006).
[26]J. Schablinski, D. Block, A. Piel, A. Melzer, H. Thomsen, H. Kählert, and M. Bonitz, "Laser heating of finite two-dimensional dust clusters: A. Experiments," Phys. Plasmas **19**, 013705 (2012).
[27]Z. Haralson and J. Goree, "Laser heating of 2-d dusty plasmas using a random arc pattern," IEEE Trans. Plasma Sci. **44**, 549–552 (2016).
[28]C.-L. Chan, W.-Y. Woon, and I. Lin, "Shear banding in mesoscopic dusty plasma liquids," Phys. Rev. Lett. **93**, 220602 (2004).
[29]C.-W. Io and I. Lin, "Steady-shear-enhanced microdiffusion with multiple time scales of confined, mesoscopic, two-dimensional dusty-plasma liquids," Phys. Rev. E **80**, 036401 (2009).
[30]V. Nosenko, A. V. Ivlev, and G. E. Morfill, "Microstructure of a liquid two-dimensional dusty plasma under shear," Phys. Rev. Lett. **108**, 135005 (2012).
[31]F. Irgens, *Rheology and Non-Newtonian Fluids* (Springer International Publishing, New York, 2014).
[32]W.-T. Juan, M.-H. Chen, and I. Lin, "Nonlinear transports and microvortex excitations in sheared quasi-two-dimensional dust Coulomb liquids," Phys. Rev. E **64**, 016402 (2001).
[33]A. Gavrikov, I. Shakhova, A. Ivanov, O. Petrov, N. Vorona, and V. Fortov, "Experimental study of Laminar flow in dusty plasma liquid," Phys. Lett. A **336**, 378–383 (2005).
[34]N. A. Vorona, A. V. Gavrikov, A. S. Ivanov, O. F. Petrov, V. E. Fortov, and I. A. Shakhova, "Viscosity of a dusty plasma liquid," J. Exp. Theor. Phys. **105**, 824–830 (2007).
[35]A. V. Ivlev, V. Steinberg, R. Kompaneets, H. Höfner, I. Sidorenko, and G. E. Morfill, "Non-Newtonian viscosity of complex-plasma fluids," Phys. Rev. Lett. **98**, 145003 (2007).
[36]O. Vaulina, O. Petrov, A. Gavrikov, X. Adamovich, and V. Fortov, "Experimental study of transport of macroparticles in plasma rf-discharge," Phys. Lett. A **372**, 1096–1100 (2008).
[37]V. E. Fortov, O. F. Petrov, O. S. Vaulina, and R. A. Timirkhanov, "Viscosity of a strongly coupled dust component in a weakly ionized plasma," Phys. Rev. Lett. **109**, 055002 (2012).
[38]V. Nosenko, A. V. Ivlev, and G. E. Morfill, "Anisotropic shear melting and recrystallization of a two-dimensional complex plasma," Phys. Rev. E **87**, 043115 (2013).
[39]V. Nosenko and J. Goree, "Shear flows and shear viscosity in a two-dimensional Yukawa system (dusty plasma)," Phys. Rev. Lett. **93**, 155004 (2004).
[40]P. Hartmann, M. C. Sándor, A. Kovács, and Z. Donkó, "Static and dynamic shear viscosity of a single-layer complex plasma," Phys. Rev. E **84**, 016404 (2011).
[41]Y. Feng, J. Goree, and B. Liu, "Observation of temperature peaks due to strong viscous heating in a dusty plasma flow," Phys. Rev. Lett. **109**, 185002 (2012).
[42]Y. Feng, J. Goree, and B. Liu, "Evolution of shear-induced melting in a dusty plasma," Phys. Rev. Lett. **104**, 165003 (2010).
[43]H. Löwen, C. P. Royall, A. Ivlev, and G. E. Morfill, "Charged colloidal suspensions and their link to complex plasmas," AIP Conf. Proc. **1397**, 201–210 (2011).
[44]Y. Feng, J. Goree, and B. Liu, "Energy transport in a shear flow of particles in a two-dimensional dusty plasma," Phys. Rev. E **86**, 056403 (2012).
[45]S. Ichimaru, "Strongly coupled plasmas: High-density classical plasmas and degenerate electron liquids," Rev. Mod. Phys. **54**, 1017–1059 (1982).
[46]Z. Donkó, J. Goree, P. Hartmann, and K. Kutasi, "Shear viscosity and shear thinning in two-dimensional Yukawa liquids," Phys. Rev. Lett. **96**, 145003 (2006).
[47]Y. Feng, J. Goree, B. Liu, and E. G. D. Cohen, "Green-kubo relation for viscosity tested using experimental data for a two-dimensional dusty plasma," Phys. Rev. E **84**, 046412 (2011).
[48]J. Pavlů, A. Velyhan, I. Richterová, Z. Němeček, J. Šafránková, I. Čermák, and P. Žilavý, "Mass-loss rate for mf resin microspheres," IEEE Trans. Plasma Sci. **32**, 704–708 (2004).
[49]J. Carstensen, H. Jung, F. Greiner, and A. Piel, "Mass changes of microparticles in a plasma observed by a phase-resolved resonance method," Phys. Plasmas **18**, 033701 (2011).
[50]M. Mikikian, L. Boufendi, A. Bouchoule, H. M. Thomas, G. E. Morfill, A. P. Nefedov, V. E. Fortov, and PKE-Nefedov Team, "Formation and behaviour of dust particle clouds in a radio-frequency discharge: Results in the laboratory and under microgravity conditions," New J. Phys. **5**, 19 (2003).
[51]Such a mass loss was demonstrated by Pavlů *et al.*[48] using MF microspheres charged by an electron beam in a Paul trap (without a plasma), and by Carstensen *et al.*[49] using an argon plasma. In both experiments, a mass loss was observed, and attributed mainly to outgassing of the volatile components of the particles, in a way similar to what is observed by baking them at high temperature in a vacuum. Another process, sputtering, can cause the mass to either increase or decrease, depending on what is

sputtered. In the high-power plasma of Carstensen *et al*., the mass can increase due to sputtering of the electrode surface, leading to a constant deposition of electrode material on the particles. On the other hand, in a low-power plasma the particles themselves can be eroded by sputtering, as shown by Mikikian *et al*.[50]

[52]B. Liu and J. Goree, "Superdiffusion and non-Gaussian statistics in a driven-dissipative 2d dusty plasma," Phys. Rev. Lett. **100**, 055003 (2008).

[53]B. L. Holian, A. F. Voter, and R. Ravelo, "Thermostatted molecular dynamics: How to avoid the Toda demon hidden in Nosé-Hoover dynamics," Phys. Rev. E **52**, 2338–2347 (1995).

[54]We chose the search radius as half the particle spacing, which was about 39–40 pixels, depending on the run. This choice was based on a tradeoff between losing track of particles with too small a search radius and being unable to distinguish between multiple found particles with too large a search radius.

[55]S. Nunomura, J. Goree, S. Hu, X. Wang, A. Bhattacharjee, and K. Avinash, "Phonon spectrum in a plasma crystal," Phys. Rev. Lett. **89**, 035001 (2002).

[56]Z. Donkó, G. J. Kalman, and P. Hartmann, "Dynamical correlations and collective excitations of Yukawa liquids," J. Phys.: Condens. Matter **20**, 413101 (2008).

[57]X. Wang, A. Bhattacharjee, and S. Hu, "Longitudinal and transverse waves in Yukawa crystals," Phys. Rev. Lett. **86**, 2569–2572 (2001).

[58]W. H. Press, S. A. Teukolsky, W. T. Vetterling, and B. P. Flannery, *Numerical Recipes in C: The Art of Scientific Computing*, 2nd ed. (Cambridge University Press, New York, 1992).

[59]To quantify the percentage error in viscosity due to the uncertainties of ω_{pd} and κ, we repeated our entire analysis of Eqs. (7)–(9) for various pairs of ω_{pd} and κ. These pairs were chosen to be on the outermost contour of Fig. 4, which corresponds to a one-sigma uncertainty for two parameters.

[60]C. K. Birdsall and A. B. Langdon, *Plasma Physics via Computer Simulation* (IOP Publishing Ltd., New York, 1991).

[61]P. Hartmann, G. J. Kalman, Z. Donkó, and K. Kutasi, "Equilibrium properties and phase diagram of two-dimensional Yukawa systems," Phys. Rev. E **72**, 026409 (2005).

[62]Extending our experimental method to lower values of Γ would face some technical challenges. We expect Γ to increase with the mass density of the material our particles are made of, so that a lower mass density would be attractive for achieving a lower Γ. Unfortunately, particles made of material with a density much smaller than our melamine formaldehyde are not readily available. A decrease in Γ could also be achieved by reducing the area of the heating region, but this would compromise the uniformity of the temperature profile. Finally, operating at a lower gas pressure would allow achieving a lower Γ, but with such a lower gas pressure we would be unable to operate with a stable crystal as required for determining ω_{pd} and κ.

[63]K. Y. Sanbonmatsu and M. S. Murillo, "Shear viscosity of strongly coupled Yukawa systems on finite length scales," Phys. Rev. Lett. **86**, 1215–1218 (2001).

[64]B. Liu and J. Goree, "Shear viscosity of two-dimensional Yukawa systems in the liquid state," Phys. Rev. Lett. **94**, 185002 (2005).

[65]T. S. Ramazanov and K. N. Dzhumagulova, "Shear viscosity of dusty plasma obtained on the basis of the Langevin dynamics," Contrib. Plasma Phys. **48**, 357–360 (2008).